Simultaneous Segmentation and Classification of Mass Region From Mammograms Using a Mixed-Supervision Guided Deep Model

Tianyu Shen, Chao Gou, *Member, IEEE*, Jiangong Wang, and Fei-Yue Wang, *Fellow, IEEE*

***Abstract*—Automatic diagnosis based on medical imaging necessitates both lesion segmentation and disease classification. Lesion segmentation requires pixel-level annotations while disease classification only requires image-level annotations. The two tasks are usually studied separately despite the latter problem relies on the former. Motivated by the close correlation between them, we propose a mixed-supervision guided method and a residual-aided classification U-Net model (ResCU-Net) for joint segmentation and benign-malignant classification. By coupling the strong supervision in the form of segmentation mask and weak supervision in the form of benign-malignant label through a simple annotation procedure, our method efficiently segments tumor regions while simultaneously predicting a discriminative map for identifying the benign-malignant types of tumors. Our network, ResCU-Net, extends U-Net by incorporating the residual module and the SegNet architecture to exploit multilevel information for achieving improved tissue identification. With experiments on a public mammogram database of INbreast, we validate the effectiveness of our method and achieve consistent improvements over state-of-the-art models.**

***Index Terms*—Mixed-supervision, deep learning, segmentation and classification, mammogram.**

I. Introduction

BREAST cancer is one of the major forms of cancer among women worldwide. Recent statistical results show that breast cancer accounts for 30% of estimated new cases and 14% of deaths [1] among all the cancers of the highest level. Early detection and diagnosis of breast cancer are critical for increasing treatment options and the survival of patients. Digital X-ray mammography enables direct imaging of morphological breast tissue and has become an essential imaging modality for breast cancer diagnosis. However, manual breast mass segmentation or classification is time consuming and prone to human errors. Automatic segmentation and classification to distinguish breast cancer as either benign or malignant of mass in mammograms can assist radiologists in the accurate diagnosis and clinical treatment.

There are primarily two challenges for breast mass segmentation and classification in mammograms. Firstly, it is difficult to generalize a specific and precise segmentation method suitable for all phenotypic categories, because of the large variations of the masses in terms of texture and location in the mammogram with low contrast, ambiguous boundaries and strong noise [2]. Secondly, for breast mass classification, a method with high performance is expected to have a desirable ability to distinguish between benign and malignant mass abnormalities, which associate with strong irregularities of mass shape, size and density [3].

In earlier studies involving mass segmentation, region growing [4], active contour [5], [6] and Markov random field (MRF) methods [7] are some of the commonly used methods for automatic breast mass segmentation in mammograms. As for mass classification, most of conventional studies focus on utilizing a set of hand-crafted or semi-automatic features, such as texture, shape and margin features, to describe the characteristics of masses. Then machine learning classifiers, such as support vector machines (SVM), fuzzy C-Mean clustering (FCM), decision tree, K-nearest neighbor (KNN) and so on, are built based on these selected features [8], [9]. However, these methods cannot achieve an excellent performance for mass segmentation or classification, because the hand-crafted features depending on prior knowledge have difficulty in handling complex shape variations and texture distribution between the masses and surrounding tissues.

With the significant breakthrough of deep learning (DL) methods in a wide range of computer vision applications [10]–[12], recent studies focus on utilizing deep convolutional neural networks (DCNN) to achieve end-to-end mass segmentation or classification based on automatically extracted deep high-level features, which overcome the limitation of artificial designed features and produce state-of-the-art performance in biomedical image community [13]–[16]. The mostly used CNN models for biomedical image segmentation include the fully convolutional network (FCN) [17], SegNet [18] and U-Net [13]. And various DCNN-based architectures have been proposed to diagnose a disease by classifying its severity [14], [15], [19]–[21]. Also, the DL models have been applied to X-ray mammography

Manuscript received November 11, 2019; revised December 19, 2019; accepted December 21, 2019. Date of publication December 31, 2019; date of current version January 31, 2020. This work was supported in part by the National Natural Science Foundation of China under Grants 61806198 and 61533019. The associate editor coordinating the review of this manuscript and approving it for publication was Dr. Ananda Shankar Chowdhury. *(Corresponding author: Chao Gou.)*

T. Shen and J. Wang are with the State Key Laboratory for Management and Control of Complex Systems, Institute of Automation, Chinese Academy of Sciences, Beijing 100190, China, and also with the University of Chinese Academy of Sciences, Beijing 100049, China (e-mail: shentianyu2016@ia.ac.cn; wangjiangong2018@ia.ac.cn).

C. Gou is with the School of Intelligent Systems Engineering, Sun Yat-sen University, Guangzhou 510275, China (e-mail: gouchao.cas@gmail.com).

F.-Y. Wang is with the State Key Laboratory for Management and Control of Complex Systems, Institute of Automation, Chinese Academy of Sciences, Beijing 100190, China (e-mail: feiyue.wang@ia.ac.cn).

Digital Object Identifier 10.1109/LSP.2019.2963151

1070-9908 © 2019 IEEE. Personal use is permitted, but republication/redistribution requires IEEE permission.
See https://www.ieee.org/publications/rights/index.html for more information.

Authorized licensed use limited to: INSTITUTE OF AUTOMATION CAS. Downloaded on July 23,2020 at 04:17:44 UTC from IEEE Xplore. Restrictions apply.

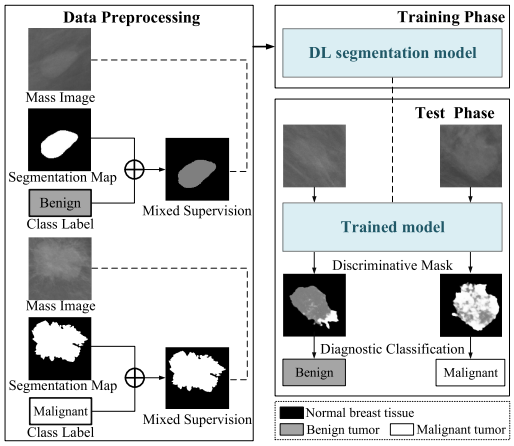

Fig. 1. Mixed-supervision guided pipeline for simultaneous lesion segmentation and benign-malignant classification of breast mass in mammograms. We enable mixed supervision through a combination of strong supervision in the form of segmentation maps and weak supervision in the form of class label.

image analysis in lesion segmentation [22]–[25] and breast mass classification [21], [26]–[29].

According to clinical experience, lesion segmentation and benign-malignant classification for breast mass in mammograms utilize similar features such as breast density, texture, mass shape and margin. However, there is rarely a simple and efficient way to achieve simultaneous end-to-end segmentation and classification of mass while maintaining desirable accuracy and efficiency. This work is motivated towards developing a simple and efficient DL technique that performs joint mass segmentation and classification of mass with favorable performance. In this context, a conceptually simple method based on mixed-supervision is presented and a residual-aided classification U-Net model (ResCU-Net) incorporating the SegNet architecture is proposed. We apply the mixed-supervision in several existing DL segmentation models and proposed ResCU-Net, by coupling strong supervision with weak supervision through low-cost input in the form of segmentation mask and benign-malignant label. Experimental comparisons are conducted on INbreast dataset [30].

The main contributions of our paper include: (1) We introduce a novel mixed-supervision guided method, which can be applied in common segmentation models and enable predicting a discriminative mask for simultaneous segmentation and classification of mass. (2) We propose a deep model named ResCU-Net by extending U-Net with the residual module and the SegNet architecture for better multilevel feature extraction. (3) Quantitative and qualitative experiments on INbreast database demonstrate the effectiveness of proposed method in both segmentation and classification compared with other state-of-the-art work.

II. Method and Model

A. Mixed-Supervision Guided Pipeline

We present a mixed-supervision guided pipeline (Fig. 1) composed of an automatic data preprocessing phase, model training phase and testing phase for simultaneous end-to-end mass segmentation and classification of mammograms.

In the data preprocessing phase, all of the masks are automatically filled with three grayscale levels based on their corresponding category labels. The white, gray and black pixels

Algorithm 1: Framework of Double Threshold Algorithm.

Input: grayscale mask M; $min\lambda = 0$; $max\lambda = 255$
Initialization: $N_0, N_1, N_2, N_3, S_0, S_1, S_2, S_3 \leftarrow 0$;
for $\lambda_1(i) \in [min\lambda, max\lambda]$, $\lambda_2(j) \in [min\lambda, max\lambda]$ **do**
  for *each pixel* $p \in M$ **do**
    if *grayvalue(p)* $\in [0, \lambda_1(i)]$ **then**
      $N_0 \leftarrow N_0 + 1; S_0 \leftarrow S_0 + grayvalue(p)$
    else if *grayvalue(p)* $\in (\lambda_1(i), 255]$ **then**
      $N_1 \leftarrow N_1 + 1; S_1 \leftarrow S_1 + grayvalue(p)$
    else if *grayvalue(p)* $\in (\lambda_1(i), \lambda_2(j)]$ **then**
      $N_2 \leftarrow N_2 + 1; S_2 \leftarrow S_2 + grayvalue(p)$
    else if *grayvalue(p)* $\in (\lambda_2(j), 255]$ **then**
      $N_3 \leftarrow N_3 + 1; S_3 \leftarrow S_3 + grayvalue(p)$
  Caculate the average grayscale of different categories:
  $\mu_0 = \frac{S_0}{N_0}, \mu_1 = \frac{S_1}{N_1}, \mu_2 = \frac{S_2}{N_2}, \mu_3 = \frac{S_3}{N_3}$
  Caculate the proportion of different categories:
  $\omega_0 = \frac{N_0}{N_0 + N_1}, \omega_1 = 1 - \omega_0, \omega_2 = \frac{N_2}{N_1}, \omega_3 = \frac{N_3}{N_1}$
  Caculate the variances:
  $\sigma_1(i) = \omega_0 \cdot \omega_1 \cdot (\mu_0 - \mu_1) \cdot (\mu_0 - \mu_1)$
  $\sigma_2(i, j) = \omega_2 \cdot \omega_3 \cdot (\mu_2 - \mu_3) \cdot (\mu_2 - \mu_3)$
return $\lambda_1 = \arg\max_{\lambda_1} \sigma_1$, $\lambda_2 = \arg\max_{\lambda_2} \sigma_2$

correspond to the malignant mass region, the benign mass region and the normal breast tissue, respectively. Then, in the training phase, the processed data are used to train the deep segmentation models which are set up for three categories. In the testing phase, the models with trained parameters are used to produce the discriminative masks with category labels of test images. Finally, the resulted segmentation map and diagnostic classification category are inferred from the obtained discriminative mask (termed as M) based on a modified OTSU Threshold [31] as shown in Algorithm 1. λ_1 represents the threshold between mass and normal breast tissue, and λ_2 represents the threshold between benign and malignant lesions. That is, normal class(background), lesion class, benign class and malignant class are composed of the pixel points whose grayscale $\in [0, \lambda_1]$, $(\lambda_1, 255]$, $(\lambda_1, \lambda_2]$ and $(\lambda_2, 255]$. $N_k, S_k, \mu_k, \omega_k (k = 0, 1, 2, 3)$ denote the point number, sum of grayscale, average grayscale and proportion of the four classes, respectively. Then we caculate the inter-class variances between normal and lesion class (termed as σ_1) as well as variances between benign and malignant class (termed as σ_2). The optimal values of λ_1 and λ_2 are determined by maximizing σ_1 and σ_2. Therefore, the resulted segmentation map is determined by the binarization of M using λ_1. And The final classification decision is as follows: {the breast mass is benign, if $\omega_2 > \omega_3$; the breast mass is malignant, otherwise.}

B. ResCU-Net Model

In this work, we expect to obtain reasonably good performance simultaneously in both tasks of segmentation and classification, which is difficult for the existing deep segmentation models. Therefore, we propose a new deep model named ResCU-Net that incorporates the U-Net and SegNet architecture aided by residual block, as shown in Fig. 2.

Authorized licensed use limited to: INSTITUTE OF AUTOMATION CAS. Downloaded on July 23,2020 at 04:17:44 UTC from IEEE Xplore. Restrictions apply.

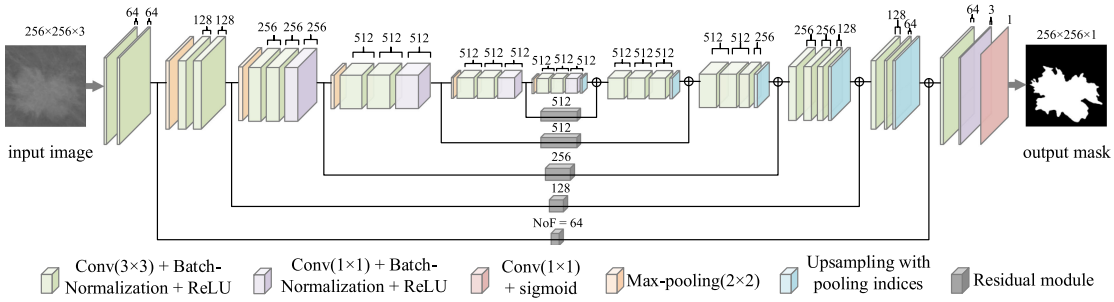

Fig. 2. The proposed ResCU-Net architecture. The upsampling operation is modified with pooling indices and the skip connections are modified with the residual modules in Fig. 3. NoF denotes the number of convolutional filters in the residual module.

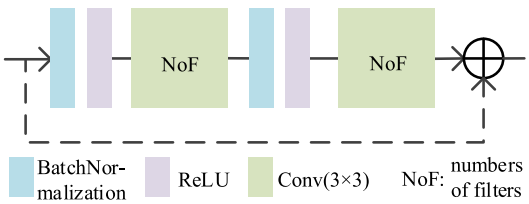

Fig. 3. Residual Module used in ResCU-Net. The module consists of two common convolution modules and a skip connection.

The SegNet [18] is an encoder-decoder architecture that adapts the VGG-16 network [32] and transfers pooling indices from encoder to decoder instead of deconvolution layers for up-sampling. The U-Net [13] architecture is also formed of encoder and decoder in general except that skip connections are added between mirrored layers in the encoder and decoder stacks to capture multilevel information.

For the problem we consider, both the segmentation task and the classification task require the model to be able to extract deeper features concerning mass shape and margin. However, these features would be easily lost in the usual encoder-decoder networks, in which all the information flows through every single layer.

The proposed ResCU-Net applies the VGG-16 architecture with pooling indices inspired from SegNet and skip connections from U-Net to capture all of necessary features and congregate them to output pixel-wise probabilistic predictions. This integrated structure convergences faster during training and achieves a fairly good segmentation performance while reducing the reliance on massive training data. Also, the skip connections are ameliorated by applying the residual modules [33] instead of straight-forward cropping and copying. Thus the depth of feature maps is increased and both high-level features and low-level features are extracted. The adopted residual module is shown in Fig. 3. It can be defined as:

$$\mathbf{y} = \mathcal{F}\left(\mathbf{x}, \{W_i\}\right) + \mathbf{x} \tag{1}$$

where $\mathbf{x}$ and $\mathbf{y}$ are the input and output vectors of the module. $\{W_i\}$ represents the parameter set to be learned in the residual mapping $\mathcal{F}$. Actually, the essence of residual network is equal to ensemble learning. This improved skip connection promotes the feature extraction capability of the network with a relatively small increase in the quantity of parameters. Furthermore, 1×1 convolutions are adopted in some layers to increase the number of channels and nonlinearity of the decision function [32].

The energy function is computed by a pixel-wise sigmoid function over the final feature map combined with the cross-entropy loss function as defined as:

$$\mathcal{L}_{mce} = \frac{1}{n}\sum_i \left(y_i \cdot \ln\left(\hat{y}_i\right) + \left(1 - y_i\right) \cdot \ln\left(1 - \hat{y}_i\right)\right) \tag{2}$$

where y represents the ground truth mask and $\hat{y}$ is the actual output map of neurons. i denotes the ith training sample and n is the number of training samples.

III. Experiments and Results

A. Dataset Description

The INbreast [30] is a public mammographic dataset including 112 breast mass images. They are cropped into 256×256 pixels size containing the mass ROI (region of interest). According to the Breast Imaging Reporting and Data System (BI-RADS) [30], 75 masses with BI-RADs$\in \{4, 5, 6\}$ are classified as malignant while 37 masses with BI-RADs$\in \{2, 3\}$ are classified as benign. We apply a 3-fold cross validation and the samples are divided into three parts with the respective number (38, 37, 37). The samples of different categories are divided as equally as possible in each fold. The training set is augmented by rotating and flipping in each fold of the experiment.

B. Implementation Details

To validate the efficacy of our proposed pipeline and ResCU-Net model, we implemented FCN, SegNet, U-Net and U-SegNet architectures to benchmark their performance on the INbreast dataset. All the models in this study are implemented based on Keras framework [34] and are tuned to achieve as good performance as possible. The final settings are as follows: the batch size is set as 8. The optimizer for updating the network parameters is stochastic gradient descent (SGD) optimizer and the learning rate is 0.01 with a decay of 1×10^{-6}. Nesterov momentum [35] with the value of 0.9 is adopted to speed up the convergence while reducing fluctuations. The number of epochs is set as 300. All training processes are performed using an NVIDIA GeForce GTX 1080Ti GPU.

C. Results and Discussion

The segmentation performance is evaluated by overall accuracy (Acc.), sensitivity (Sen.), specificity (Spe.), Dice coefficient, Jaccard index (Jac.) and MCC Matthews correlation coefficient (MCC) as shown in Table I, while the classification performance is analyzed by measurement metrics including

Authorized licensed use limited to: INSTITUTE OF AUTOMATION CAS. Downloaded on July 23,2020 at 04:17:44 UTC from IEEE Xplore. Restrictions apply.

TABLE I
SEGMENTATION PERFORMANCE OF RESCU-NET COMPARED WITH DL SEGMENTATION MODELS WITH AND WITHOUT THE MIXED-SUPERVISION (MS) STAGE ON THE INBREAST DATASET

Model	Measurement metrics(%)					
	Acc.	Sen.	Spe.	Dice	Jac.	MCC
FCN-8s [17]	91.89	**93.94**	91.63	89.42	81.25	83.28
MS-FCN-8s	92.73	93.59	92.43	90.02	82.25	84.45
SegNet [18]	91.95	91.27	93.18	89.35	81.25	83.20
MS-SegNet	93.38	91.63	94.64	90.75	83.40	85.54
U-Net [13]	91.63	87.07	**95.44**	88.76	80.13	82.32
MS-U-Net	93.18	91.77	94.31	90.52	83.03	85.22
U-SegNet [36]	84.34	87.77	83.13	80.06	68.40	68.61
MS-U-SegNet	90.52	91.90	89.77	86.87	77.69	79.99
ResCU-Net	92.91	91.51	94.64	90.50	83.02	84.99
MS-ResCU-Net	**94.16**	93.11	95.02	**91.78**	**85.13**	**87.22**

TABLE II
CLASSIFICATION PERFORMANCE OF MIXED-SUPERVISION GUIDED RESCU-NET COMPARED WITH MIXED-SUPERVISION GUIDED DL SEGMENTATION MODELS ON INBREAST DATASET

Model	Measurement metrics (%)				
	Acc.	Recall(Sen.)	Spe.	Precision	F1-score
MS-FCN-8s	86.76	87.80	85.19	90.00	88.89
MS-SegNet	88.24	85.37	**92.59**	**94.59**	89.74
MS-U-Net	80.88	78.05	85.19	88.89	83.12
MS-U-SegNet	88.24	95.12	77.78	86.67	90.70
MS-ResCU-Net	**94.12**	**97.56**	88.89	93.02	**95.24**

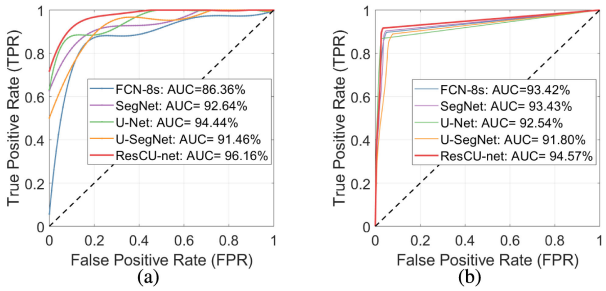

Fig. 4. The performance comparison among mixed-supervision guided ResCU-Net and DL segmentation models in terms of ROC curves and AUC values on INbreast Dataset: (a) classification, (b) segmentation.

overall accuracy, recall (sensitivity), specificity, precision and F1-score as shown in Table II. It can be observed that the segmentation performance of the DL models is improved through the addition of mixed-supervision. And mixed-supervision guided ResCU-Net gives the best segmentation and classification performance on the whole. Also, receiver operating characteristic (ROC) curves and their AUCs (Area Under the Curve) are adopted to evaluate the performance using different thresholds λ_1 and λ_2 (mentioned in Section II-A) as shown in Fig. 4. ROC curve is produced by a tradeoff between sensitivity and specificity in a two-dimensional plane. Although ResCU-Net does not perform the best at certain specific thresholds, it does the best overall with an AUC of 96.16% for classification and 94.57% for segmentation. In Fig. 5, some visual results for MS-ResCU-Net compared with other models on INbreast are shown. It can be observed that the proposed model is capable of not only correcting misclassified pixels in tumor regions but also providing better segmentation boundaries and masks. Furthermore, evaluations of Dice, overall accuracy and AUC

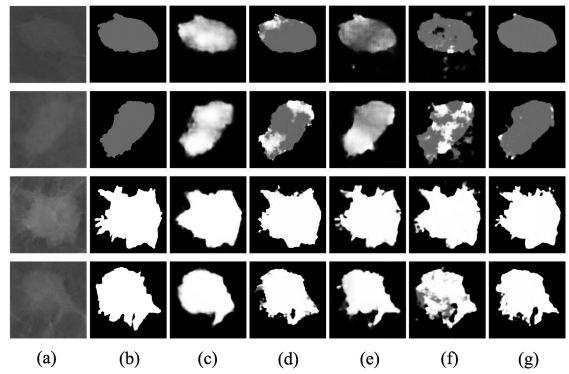

Fig. 5. Visualization of results for segmentation and classification on the INbreast Dataset: (a) Input mass image, (b) Ground truth mask in the form of mixed-supervision, (c) MS-FCN-8 s, (d) MS-SegNet, (e) MS-U-Net, (f) MS-U-SegNet, (g) Proposed MS-ResCU-Net.

TABLE III
SEGMENTATION PERFORMANCE OF MS-RESCU-NET COMPARED WITH STATE-OF-THE-ART METHODS ON INBREAST DATASET

Model	Dice(%)	AUC(%)
Dhungel et. al. [22]	90.00	N/A
Dhungel et al. [28]	85.00	91.00
Zhu et. al. [24]	89.36	91.27
Cardoso et al. [37]	88.00	N/A
Wang et. al. [38]	91.10	N/A
MS-ResCU-Net	**91.78**	**94.57**

TABLE IV
CLASSIFICATION PERFORMANCE OF MS-RESCU-NET COMPARED WITH WTATE-OF-THE-ART METHODS ON INBREAST DATASET

Model	Acc.(%)	AUC(%)
Dhungel et al. [26]	91.00	N/A
Zhu et al. [27]	90.00	89.00
Dhungel et al. [28]	91.00	76.00
Carneiro et al. [29]	N/A	90.00
Shams et al. [21]	93.50	92.50
MS-ResCU-Net	**94.12**	**96.16**

value are compared with related mass segmentation and classification works on mammograms, as shown in Table III and Table IV. Mixed-supervision guided ResCU-Net achieves the best segmentation and classification performance with the Dice of 91.78% and the overall accuracy of 94.12% on the INbreast Dataset.

IV. CONCLUSION

Lesion segmentation and benign-malignant classification in mammograms are important for the automatic diagnosis of breast cancer. Motivated by the fact that the two tasks utilize essentially similar features, we present a mixed-supervision guided pipeline for simultaneous mass segmentation and classification. To address the challenge that the existing models cannot provide reasonably good performance in both tasks, we further propose a residual-aided classification U-Net model (ResCU-Net). Experimental results on INbreast show the proposed MS-ResCU-Net outperforms other state-of-the-art approaches on both segmentation and classification tasks. In the future, we will further investigate the improvement of model architecture, such as the fusion of adversarial structure or graph model, to handle the cases with bad performance.

Authorized licensed use limited to: INSTITUTE OF AUTOMATION CAS. Downloaded on July 23,2020 at 04:17:44 UTC from IEEE Xplore. Restrictions apply.

REFERENCES

[1] R. L. Siegel, K. D. Miller, and A. Jemal, "Cancer statistics," *CA: A Cancer J. Clin.*, vol. 68, no. 1, p. 730, 2018.

[2] Y. Wang, D. Tao, X. Gao, X. Li, and B. Wang, "Mammographic mass segmentation: Embedding multiple features in vector-valued level set in ambiguous regions," *Pattern Recognit.*, vol. 44, no. 9, pp. 1903–1915, 2011.

[3] H. Li, X. Meng, T. Wang, Y. Tang, and Y. Yin, "Breast masses in mammography classification with local contour features," *Biomed. Eng. Online*, vol. 16, no. 1, p. 44, 2017.

[4] N. Petrick, H. P. Chan, B. Sahiner, and M. A. Helvie, "Combined adaptive enhancement and region-growing segmentation of breast masses on digitized mammograms," *Med. Phys.*, vol. 26, no. 8, pp. 1642–1654, 1999.

[5] P. Rahmati, A. Adler, and G. Hamarneh, "Mammography segmentation with maximum likelihood active contours," *Med. Image Anal.*, vol. 16, no. 6, pp. 1167–1186, 2012.

[6] Y. Yuan, M. L. Giger, H. Li, K. Suzuki, and C. Sennett, "A dual-stage method for lesion segmentation on digital mammograms," *Med. Phys.*, vol. 34, no. 11, pp. 4180–4193, 2007.

[7] C. D'Elia, C. Marrocco, M. Molinara, G. Poggi, G. Scarpa, and F. Tortorella, "Detection of microcalcifications clusters in mammograms through ts-mrf segmentation and svm-based classification," in *Proc. IEEE 17th Int. Conf. Pattern Recognit.*, 2004, vol. 3, pp. 742–745.

[8] X. Liu and J. Tang, "Mass classification in mammograms using selected geometry and texture features, and a new svm-based feature selection method," *IEEE Syst. J.*, vol. 8, no. 3, pp. 910–920, Sep. 2014.

[9] B. Surendiran and A. Vadivel, "A hybrid classifier for mammogram mass classification using various new geometric shape and margin features," *Int. J. Rapid Manuf.*, vol. 2, no. 1/2, pp. 56, 2011.

[10] K. F. Wang, C. Gou, and F.-Y. Wang, "Parallel vision: An acp-based approach to intelligent vision computing," *Acta Automatica Sinica*, vol. 42, no. 10, pp. 1490–1500, 2016.

[11] L. Li, Y. Lin, N. Zheng, and F.-Y. Wang, "Parallel learning: A perspective and a framework," *IEEE/CAA J. Automatica Sinica*, vol. 4, no. 3, pp. 389–395, 2017.

[12] C. Gou, H. Zhang, K. F. Wang, F.-Y. Wang, and Q. Ji, "Cascade learning from adversarial synthetic images for accurate pupil detection," *Pattern Recognit.*, vol. 88, pp. 584–594, 2019.

[13] O. Ronneberger, P. Fischer, and T. Brox, "U-net: Convolutional networks for biomedical image segmentation," in *Proc. Int. Conf. Med. Image Comput. Comput. Assisted Intervention*, 2015, pp. 234–241.

[14] L. Huang, X. He, L. Fang, H. Rabbani, and X. Chen, "Automatic classification of retinal optical coherence tomography images with layer guided convolutional neural network," *IEEE Signal Process. Lett.*, vol. 26, no. 7, pp. 1026–1030, Jul. 2019.

[15] Y. Zhou *et al.*, "Collaborative learning of semi-supervised segmentation and classification for medical images," in *Proc. Conf. Comput. Vis. Pattern Recognit.*, 2019.

[16] W. Du, H. Chen, P. Liao, H. Yang, G. Wang, and Y. Zhang, "Visual attention network for low-dose ct," *IEEE Signal Process. Lett.*, vol. 26, no. 8, pp. 1152–1156, Aug. 2019.

[17] J. Long, E. Shelhamer, and T. Darrell, "Fully convolutional networks for semantic segmentation," in *Proc. Conf. Comput. Vis. and Pattern Recognit*, 2015, pp. 3431–3440.

[18] V. Badrinarayanan, A. Kendall, and R. Cipolla, "Segnet: A deep convolutional encoder-decoder architecture for image segmentation," *IEEE Trans. Pattern Anal. Mach. Intell.*, vol. 39, no. 12, pp. 2481–2495, Dec. 2017.

[19] Y. Yang, T. Li, W. Li, H. Wu, W. Fan, and W. Zhang, "Lesion detection and grading of diabetic retinopathy via two-stages deep convolutional neural networks," in *Proc. Int. Conf. Med. Image Comput. Comput. Assisted Intervention Soc.*, 2017, pp. 533–540.

[20] Z. Qin, Z. Jiang, J. Chen, C. Hu, and Y. Ma, 'Semg-based tremor severity evaluation for parkinson's disease using a light-weight cnn," *IEEE Signal Process. Lett.*, vol. 26, no. 4, pp. 637–641, Apr. 2019.

[21] S. Shams, R. Platania, J. Zhang, J. Kim, K. Lee, and S.-J. Park, "Deep generative breast cancer screening and diagnosis," in *Proc. Int. Conf. Med. Image Comput. Comput. Assisted Intervention Soc.*, 2018, pp. 859–867.

[22] N. Dhungel, G. Carneiro, and A. P. Bradley, "Deep learning and structured prediction for the segmentation of mass in mammograms," in *Proc. Int. Conf. Med. Image Comput. Comput. Assisted Intervention Soc.*, 2015.

[23] N. Dhungel, G. Carneiro, and A. P. Bradley, "Deep structured learning for mass segmentation from mammograms," in *Proc. Int. Conf. Image Process.* 2015, pp. 2950–2954.

[24] W. Zhu, X. Xiang, T. D. Tran, G. D. Hager, and X. Xie, "Adversarial deep structured nets for mass segmentation from mammograms," in *Proc. Int. Symp. Biomed. Imag*, 2018, pp. 847–850.

[25] T. Shen, C. Gou, F.-Y. Wang, Z. He, and W. Chen, "Learning from adversarial medical images for x-ray breast mass segmentation," *Comput. Methods Programs Biomed.*, vol. 180, 2019, Art. no. 105012.

[26] N. Dhungel, G. Carneiro, and A. P. Bradley, "The automated learning of deep features for breast mass classification from mammograms," in *Proc. Int. Conf. Med. Image Comput. Comput. Assisted Intervention Soc.*, 2016, pp. 106–114.

[27] W. Zhu, Q. Lou, Y. S. Vang, and X. Xie, "Deep multi-instance networks with sparse label assignment for whole mammogram classification," in *Proc. Int. Conf. Med. Image Comput. Comput. Assisted Intervention Soc.*, 2017, pp. 603–611.

[28] N. Dhungel, G. Carneiro, and A. P. Bradley, "A deep learning approach for the analysis of masses in mammograms with minimal user intervention," *Med. Image Anal.*, vol. 37, pp. 114–128, 2017.

[29] G. Carneiro, J. Nascimento, and A. P. Bradley, "Automated analysis of unregistered multi-view mammograms with deep learning," *IEEE Trans. Med. Imag.*, vol. 36, no. 11, pp. 2355–2365, Nov. 2017.

[30] I. Moreira, I. Amaral, I. Domingues, A. Cardoso, M. Cardoso, and J. Cardoso, "Inbreast: Toward a full-field digital mammographic database," *Acad. Radiol.*, vol. 19, no. 2, pp. 19, 2012.

[31] N.A. Otsu, "A threshold selection method from gray-level histograms," *IEEE Trans. Syst. Man Cybern.*, vol. SMC-9, no. 1, pp. 62–66, Jan. 1979.

[32] K. Simonyan and A. Zisserman, "Very deep convolutional networks for large-scale image recognition," *CoRR*, vol. abs/1409.1556, 2014.

[33] K. He, X. Zhang, S. Ren, and J. Sun, "Deep residual learning for image recognition," in *Proc. IEEE Conf. Comput. Pattern Recognit.* Jun. 2016, pp. 770–778.

[34] F. Chollet *et al.*, "Keras," 2015. [Online]. Available: https://keras.io

[35] I. Sutskever, J. Martens, G. Dahl, and G. Hinton, "On the importance of initialization and momentum in deep learning," in *Proc. Int. Conf. Mach. Learn.*, Jun. 2013.

[36] P. Kumar, P. Nagar, C. Arora, and A. Gupta, "U-segnet: Fully convolutional neural network based automated brain tissue segmentation tool," in *Proc. IEEE Int. Conf. Image Process.*, 2018, pp. 3503–3507.

[37] J. S. Cardoso, I. Domingues, and H. P. Oliveira, "Closed shortest path in the original coordinates with an application to breast cancer," *Int. J. Pattern Recognit. Artif. Intell.*, vol. 29, no. 1, 2015, Art. no. 1555002.

[38] R. Wang *et al.*, "Multi-level nested pyramid network for mass segmentation in mammograms," *Neurocomputing*, vol. 363, pp. 313–320, 2019.

Authorized licensed use limited to: INSTITUTE OF AUTOMATION CAS. Downloaded on July 23,2020 at 04:17:44 UTC from IEEE Xplore. Restrictions apply.